International Journal of Concrete Structures and Materials
Vol.10, No.4, pp.527–537, December 2016
DOI 10.1007/s40069-016-0166-3
ISSN 1976-0485 / eISSN 2234-1315

A Study on Mechanical Properties of Porous Concrete Using Cementless Binder

Jong-Won Lee[1)], Young-Il Jang[2),*], Wan-Shin Park[2)], and Sun-Woo Kim[2)]

(Received February 28, 2016, Accepted July 10, 2016, Published online August 5, 2016)

Abstract: This study evaluated the mechanical characteristics and durability of porous concrete produced with a cementless binder based on ground granulated blast furnace slag (BFS), fly ash (FA) and flue gas desulfurization gypsum (CP). As a result, the void ratio was increased slightly from the target void ratio, by 1.12–1.42 %. Through evaluating the compressive strength, it was found that the compressive strength of porous concrete with cementless binder decreased in comparison to the compressive strength of porous concrete with ordinary Portland cement (OPC), but the difference was insignificant, at 0.6–1.4 MPa. Through the freeze–thawing test to evaluate the durability, it was found that the relative dynamic elastic modulus of porous concrete with cementless binder decreased to 60 % or less at 80 cycles. The result of the chemical resistance test showed that the mass reduction rate was 12.3 % at 5 % HCl solution, and 12.7 % at 12.3 and 5 % H_2SO_4 solutions.

Keywords: cementless binder, porous concrete, industrial by-products, mechanical characteristics, durability.

1. Introduction

Phenomena such as extreme weather events and abnormal temperatures have increased drastically worldwide in recent years, and the academic theory that their cause is global warming has emerged. Meanwhile, the Durban Platform for Enhanced Action has been launched after negotiations for the adoption of a new Green House Gas (GHG) reduction system, the second commitment period of the Kyoto Protocol to the United Nations Framework Convention on Climate Change (UNFCCC) has been extended, and international agreements to reduce GHGs including negotiations on the New Climate Regime have been signed (Gartner 2004; Mehta 2001; Yang et al. 2007). Problems due to GHGs have already become serious threats to all nations around the globe and these gases are directly related to not only environmental problems but also to economic problems. Accordingly, discussions on emission trading have been taking place in relation to the reduction of GHG emissions (Oh 2005; Wu 2013).

Concrete is used in civil engineering and architectural structures including roads, bridges, dams, railroads, harbors, and water supply and sewage, which are social infrastructure, and has contributed considerably to the development of the current construction industry. However, cement, the main ingredient of concrete, not only consumes tremendous energy to reach a temperature of 1400 °C or above in its calcination process but also emits CO_2, the main GHG, on a mass scale (Malhotra 2002; Yang et al. 2007). Consequently, one of the more important fields in research in the cement industry in recent years has been research to reduce the amount of CO_2 generated by decreasing the amount of cement used. Representative among such studies is research on reducing the amount of cement used and preventing environmental pollution due to industrial byproducts by exploiting such byproducts, including BFS and FA, in place of cement (Park and Park 2005; Park et al. 2013).

Meanwhile, interest in environment blocks and planting blocks that use porous concrete with environment-friendly functions including permeation, ventilation, vegetation, water quality improvement, and sound absorption, which reduce the load on the surrounding natural environment, has increased in recent years such that these blocks have been used considerably in the construction of river revetments and levees (Lee et al. 2012). However, existing concrete is strongly alkaline due to hydrates generated by the hydration reaction of cement and water; this alkalinity has adverse effects on the environment. In particular, secondary damage has continued to emerge due to the environmental destruction of waterfront environments along rivers and the continuous elution caused by strong alkalinity.

Consequently, the present study produced cementless binder using materials such as BFS, FA, and CP as binders; the study also used scanning electron microscope (SEM) and X-ray diffractometer (XRD) analyses to confirm the types of

[1)]Department of Convergence System Engineering, Chungnam National University, Daejeon 34134, Korea.
[2)]Department of Construction Engineering Education, Chungnam National University, Daejeon 34134, Korea.
*Corresponding Author; E-mail: jang1001@cnu.ac.kr

Table 1 Physical and chemical properties of BFS.

Physical properties				
Density (g/cm^3)		Blaine (cm^2/g)		
2.90		4317		
Chemical properties				
SiO_2	Al_2O_3	Fe_2O_3	CaO	MgO
24.7	16.4	0.18	49.1	4.21

reaction products and crystalloids of porous concrete using cementless binder so as to verify porous concrete's applicability as a manufacturing and production ingredient for secondary products including concrete blocks. In addition, the study evaluated the physical and mechanical properties, such as the strength and durability, of porous concrete using cementless binder.

2. Materials and Experiment Method

2.1 Material Used

2.1.1 Cementless Binder

The mixing ratio which showed the best performance in the preliminary experiment according to the contents of admixture material was used for the cementless binder used in this study. The cementless binder premixed with admixture material improved according to the ratio using an Omni mixer was used. The physical and chemical properties of industrial by-products used for producing the cementless binder are as shown in Tables 1, 2, and 3, and the optimal ratio and physical and chemical composition of the non-cement binder produced are as shown in Tables 4 and 5.

2.1.2 Cement

The cement used for this study is ordinary Portland cement made by "A" company in Korea whose density is 3.14 g/cm^3 and Blaine fineness is 3200 cm^2/g.

2.1.3 Aggregate

Natural aggregate with a grain size of less than 5 mm was used in this study for fine aggregate and crushed granite aggregate with a grain size between 5 and 13 mm from Chungcheongnam-do Province was used for coarse aggregate. The physical characteristics of fine and coarse aggregates are as shown in Tables 6 and 7.

2.1.4 Alkali Activators

BFS and FA that are industrial by-products have almost no hydraulic property, so alkali-activator should be used to improve strength and durability (Oh et al. 2015; Criado et al. 2010). The compressive strength of mortar according to the type of alkali-activator was carried out in order to improve the strength of cementless binder. Potassium hydroxide (KOH) which showed the best strength performance as a result of experiment was used in this study, and its physical property is as shown in Table 8.

2.2 Mix Proportion and Mixing

In order to analyze the physical and mechanical properties according to the mixing factors of porous concrete using cementless binder, the target void ratio was selected as 12 and 15 %, the water-binder ratio was set to 22.5 % and the type of binder was changed to OPC and cementless binder. In order to analyze the durability, mixing was carried out with 0.3 M KOH, an alkali activation agent, and the table of mix proportion is as shown in Table 9. Also, in order to improve the dispersibility of binder paste, the split injection method was used for mixing by adding the binder and aggregates first using a 30 l Omni mixer and then mixing them with a mixer for 30 s at 50 rpm and then for 60 s at 200 rpm, and then adding mixing water and mixing them again for 180 s.

2.3 Production of Specimens

The test specimens were produced by mixing the materials in accordance with the porous concrete specimen production methods of the Technical Research Committee on Ecological Concrete in Japan, filling half of each required mold with porous concrete and compacting the concrete (JCI 2003). The test specimens were air-dry cured for 24 h, removed from the molds, and cured with a thermostat-humidistat at 20 °C in accordance with the experimental plan.

2.4 Experiment Method

2.4.1 SEM Analysis

A SEM was used to analyze the micro-structure of OPC and cementless binder samples according to their ages. Specimens for SEM analysis were taken at ages of 3, 7, 14 and 28 days from the OPC and cementless binder test blocks; the specimens were taken from the mortar portion only, without any aggregates included. The specimens' sizes were set to a maximum of 15 × 15 mm, and their heights were limited to 1 mm, which kept their total volume small. To mitigate air contact and changes in concrete, the specimens were submerged in acetone after being taken. Because the specimens consisted of cement concrete, which has particularly low electron conductivity, they were coated with 200 Å platinum and attached using silver paste. Because the samples contained substantial quantities of gas and moisture within them, an ample vacuum treatment time of 6 h was provided.

2.4.2 XRD Analysis

An XRD was used to analyze the types of substances and crystalline materials according to cementless binders age.

Table 2 Physical and chemical properties of FA.

Physical properties	
Density (g/cm^3)	Blaine (cm^2/g)
2.76	4743

Chemical properties								
SiO_2	Al_2O_3	Fe_2O_3	CaO	MgO	K_2O	TiO_2	Na_2O	P_2O_5
15.0	9.0	10.0	48.6	0.1	0.7	0.6	0.4	0.2

Table 3 Physical and chemical properties of CP.

Physical properties	
Density (g/cm^3)	Blaine (cm^2/g)
2.52	3970

Chemical properties					
SiO_2	Al_2O_3	Fe_2O_3	CaO	MgO	SO_3
1.68	0.71	0.41	60.17	0.81	21.02

Table 4 Mix proportion.

Item	Binder composition (%)					
	BFS	FA	CP	QL[a]	SL[b]	SP[c]
Cementless binder	60	20	6	8	6	0.002

[a] Quick lime, [b] slaked lime, [c] super plasticizer (powder).

Table 5 Physical and chemical properties of cementless binder.

Physical properties	
Density (g/cm^3)	Blaine (cm^2/g)
2.82	4173

Chemical properties								
SiO_2	Al_2O_3	Fe_2O_3	CaO	MgO	SO_3	K_2O	TiO_2	Na_2O
20.1	9.4	2.8	56.3	2.5	3.8	0.5	0.5	0.2

Table 6 Physical properties of natural fine aggregate.

Density (g/cm^3)	Absorption (%)	Unit weight (kg/m^3)	Fineness modulus	Sound (%)
2.59	0.8	1598	2.75	2.7

Table 7 Physical properties of coarse aggregate.

Grading (mm)	Density (g/cm^3)	Absorption (%)	Unit weight (kg/m^3)	Absolute volume (%)
5–13	2.70	0.82	1566	58.0

Table 8 Physical properties of potassium hydroxide.

Formula	Content (%)	Density (g/cm^3)	pH (0.1M)	Solubility (g/100 ml)	Molar mass (g/mol)
KOH	95	2.04	13.5	58.0	56.11

Specimens were taken only from the mortar portion of the Φ 100 × 200 mm, round-shaped test block without any aggregates included, as in the case of the specimens for the SEM analysis; specimens were then finely ground. The values obtained from X-ray diffraction were analyzed to determine the types of substances present by using

Table 9 Mix proportions of porous concrete.

Mix no.	W/B	Target void ratio (%)	Binder type	KOH (M)	Unit weight (kg/m^3)				
					B[a]	W[b]	S[c]	G[d]	Ad.[e]
1-1	22.5	12	OPC	–	405	91	205	1566	1.52
1-2			CB	–	405	91	205	1566	–
2-1		15	OPC	–	405	91	127	1566	1.52
2-2			CB	–	405	91	127	1566	–
3-1			OPC	–	405	91	127	1566	1.52
3-2			CB	0.3	405	91	127	1566	–

[a] Binder, [b] water, [c] fine aggregate, [d] coarse aggregate, [e] admixtures.

International Centre for Diffraction Data (ICDD) card numbers, which are internationally maintained by Joint Committee on Powder Diffraction Standards (JCPDS) of ASTM. The quantities of the substances were qualitatively evaluated by using the peaks of the concrete-related substances only. In addition, the types of crystalline and non-crystalline substances were analyzed and their content levels were evaluated.

2.4.3 Void Ratio Test

The void ratio was measured in accordance with the "Testing Method for Void Ratio of Porous Concrete (draft)" in the "report of the research committee related to the establishment of design and construction method for porous concrete" (JCI 2003) of the Japan Concrete Institute. The void ratio was calculated using the following equation (1).

$$A_t\ (\%) = \left\{1 - \frac{(W_2 - W_1)}{V}\right\} \times 100 \tag{1}$$

where A_t is the total void ratio of the porous concrete (%), W_1 is the weight of the test piece in water (g), W_2 is the air dried weight of the test piece after being placed in natural conditions for 24 h (g), and V is the volume of the test piece (cm^3).

2.4.4 Compressive Strength Test

For tests on the compressive strength, specimens of Ø 100 mm × 200 mm were made and then cured under water at 20 ± 2 °C for 28 days. Measurements were taken in accordance with the KS F 2405 "Test Method for Compressive Strength of Concrete" using the UTM made by "W" company in Korea.

2.4.5 Freezing–Thawing Test

As for freezing–thawing tests, freezing–thawing was evaluated in accordance with method A (rapid underwater freezing–thawing tests) in KS F 2456 "Testing Method for Resistance of Concrete to Rapid Freezing–Thawing". After curing in an underwater environment of 20 ± 2 °C up to the age of 14 days, the relative dynamic modulus of elasticity was measured every 30 cycles by the dynamic modulus of elasticity measurement device was calculated by using the following equation (2).

$$p_c = \frac{(n_1)^2}{(n)^2} \times 100 \tag{2}$$

where P_c is the relative dynamic modulus of elasticity, after C cycles of freezing and thawing (%), n is the fundamental transverse frequency at 0 cycles of freezing and thawing, and n_1 is the fundamental transverse frequency after C cycles of freezing and thawing.

2.4.6 Chemical Resistance Test

Chemical resistance tests were performed in accordance with the test methods in ASTM C 267-01 "Standard Test Method for Chemical Resistance of Mortars, Grouts, and Monolithic Surfacings and Polymer Concretes". After curing in a wet state at 20 ± 2 °C for 28 days, the specimens were immersed for 84 days in a 5 % HCl solution and a 5 % H_2SO_4, respectively. After 3, 7, 14, 28, 56, and 84 days, the specimens were taken out, washed with tap water to remove the eroded and scaled parts, and dried in air to measure the mass change rate was calculated using the following equation (3).

$$\text{Mass loss}\ (\%) = \frac{W - C}{C} \times 100 \tag{3}$$

where C is the conditioned weight of the specimen (g), and W is the weight of specimen after immersion (g).

3. Results and Discussion

3.1 SEM

Figures 1 and 2 show the results of the SEM images of OPC and cementless binder according to material age. At early ages, a number of new crystalline structures in the mineral kingdom were found in cementless binder rather than in OPC; these were: Gismondine, with the chemical formula $CaAl_2Si_2O_8{\cdot}4[H_2O]$; Hatrurite, with the chemical formula $Ca_3(SiO_4)O$; and Wollastonite, with the chemical formula $NaAlSi_3O_8$. These structures are believed to have been formed during the process of chemical properties such CaO, Al_2O_3 and SiO_2 contained in BFS, CP, and quicklime that comprise cementless binder, forming an

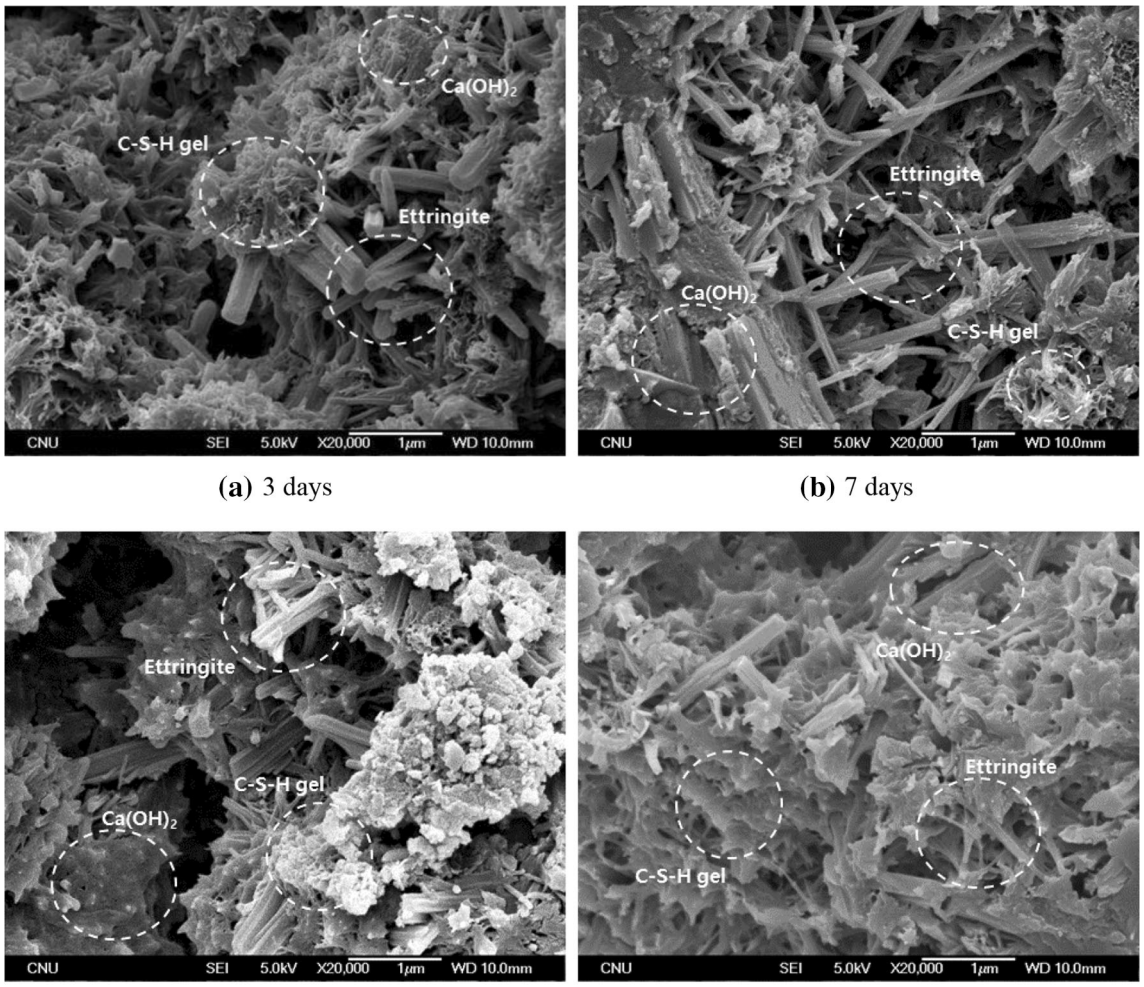

(a) 3 days **(b)** 7 days

(c) 14 days **(d)** 28 days

Fig. 1 SEM images of OPC porous concrete.

$Al_2O_3 \cdot SiO_2 \cdot 6H_2O$ (ASH_6) hydrate, which is a film about 0.2 μm thick, and which then ruptures upon contact with the OH properties of slaked lime, thereby eluting Si_4^+ and Al_3^+ ions (Pacheco-Torgal 1991; Brough and Atkinson 2002; Puertas and Fernández-Jiménez 2003; Kumar et al. 2010; Kathirvel 2016). This result is presumably attributable to the fact that, in cementless binder Porous concrete, $2CaO \cdot Al_2O_3 \cdot SiO_2$, an amorphous substance, undergoes a hydration reaction unlike the hydration reaction of existing OPC. This kind of result is also believed to affect the formation of Ettringite. In particular, OPC's Ettringite's chemical formula is $C_3A \cdot 3CaSO_4 \cdot 32H_2O$, whereas cementless binders Ettringite chemical formula is $Ca_6Al_2(SO_4)_3(OH)_{12}(H_2O)_{26}$, and its hydration reaction of amorphous substance is believed to have led to this outcome. It takes a longer time for cementless binder to form Ettringite, $Ca(OH)_2$ and C–S–H gel than it does for OPC, but the formation starts to become more active after the age of 14 days; and, from 28 days, the density of the microstructures and structures reaches a level similar to that of OPC.

3.2 XRD

Figures 3, 4, 5, 6, and 7 shows the results of the XRD analysis of OPC and cementless binder according to material age. The crystalloids of porous concrete using cementless binders were fewer than those of porous concrete using OPC by approximately 12 %. However, at the age of 28 days, the crystalloids of porous concrete using cementless binders amounted to 62 %, thus increasing by approximately 10 % in comparison with the early stage, and differed quantitatively from those of porous concrete using OPC by approximately 8 %, thus exhibiting outstanding crystalloid generation. In the case of porous concrete using OPC, Ettringite, $Ca(OH)_2$, and C–S–H gel were actively generated from an early age, and the amounts of these materials generated were confirmed to increase with the passage of time (Juenger et al. 2011; Bakharev 2005). In the case of porous concrete using cementless binders, as with the results of SEM analysis, substances including Gismondine, Hatrurite, and Wollastonite were detected in considerable amounts from an early age, while the amounts of Ettringite, $Ca(OH)_2$, and C–S–H gel were relatively smaller. With the passage of time, however, the materials generated at first were no longer detected, and the amounts of Ettringite, $Ca(OH)_2$, and C–S–H gel increased.

3.3 Void Ratio

Figure 8 shows the result of target void ratio measurements of the porous concrete according to the binder type. In

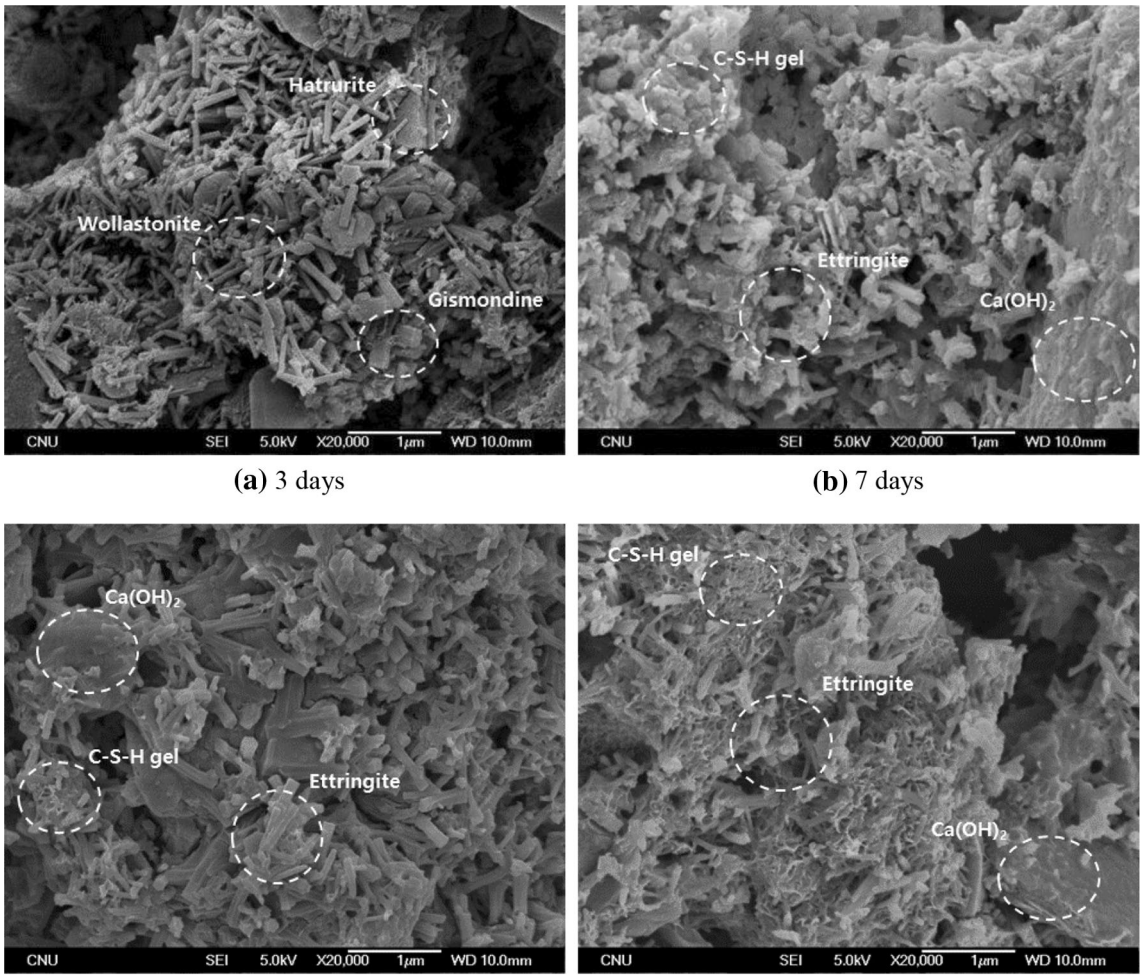

(a) 3 days **(b)** 7 days

(c) 14 days **(d)** 28 days

Fig. 2 SEM images of cementless binder porous concrete.

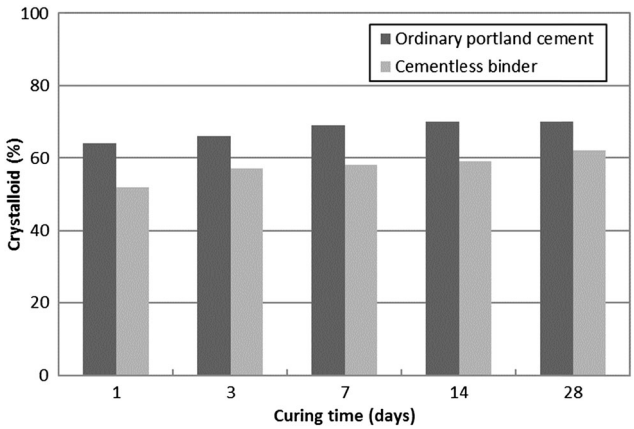

Fig. 3 Crystalloid content of the OPC and cementless binder porous concrete with different curing times.

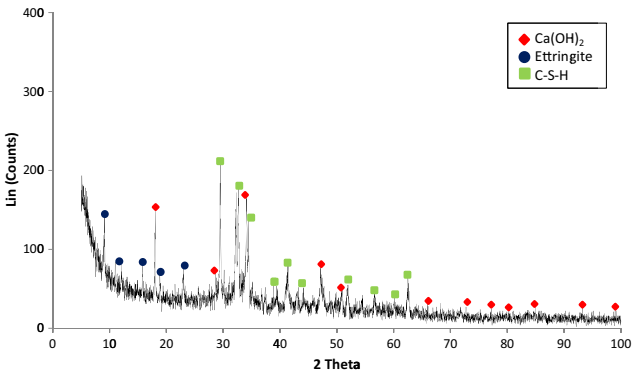

Fig. 4 XRD pattern of OPC porous concrete of 1 days of curing.

the mix design of porous concrete, the void ratio is designed as the total void ratio (target void ratio) combining the continuous voids and separate voids but continuous void become the most important factor for the main performances of porous concrete such as permeability and the provision of habitation base for living organisms. Therefore, the target void ratio and the actual void ratio (continuous voids) were compared. In the case of porous concrete using cementless binder, void ratio increased toward the target void ratio by approximately 1.12 and 1.42 % in comparison with porous concrete using OPC under all mixing conditions, the maximum difference between the actually measured void ratio and the target void ratio amounted to approximately 1.11 %, thus satisfying the target void ratio; when cementless binder with high viscosity were used, it was easier to attain the target void ratio.

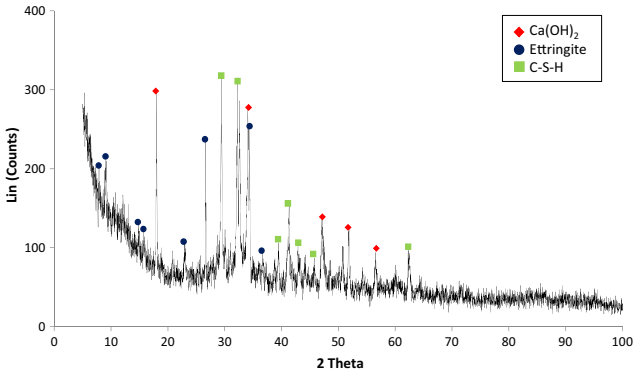

Fig. 5 XRD pattern of OPC porous concrete of 28 days of curing.

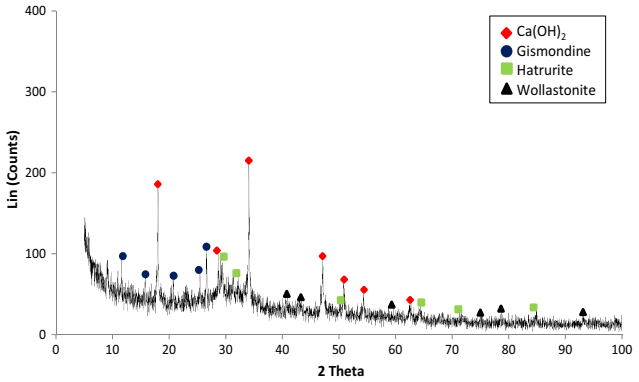

Fig. 6 XRD pattern of cementless binder porous concrete of 1 days of curing.

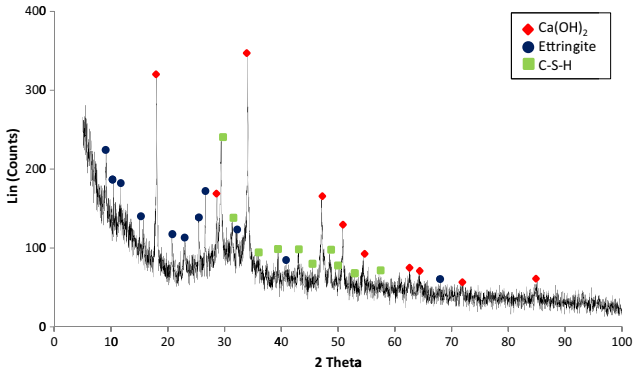

Fig. 7 XRD pattern of cementless binder porous concrete of 28 days of curing.

3.4 Compressive Strength

Figure 9 shows the test result of compressive strength of OPC and cementless binder according target void ratio porous concrete. 80 % of cementless binder used in this study consists of BFS and FA. Therefore, the initial strength of cementless binder was lower than the case of using OPC due to the latent hydraulic property of these elements. However, the strength development increased after the aging of 7 days due to improvement of alkali activation and Pozzolanic reaction between BFS and FA. When the compressive strength properties were examined, it was found that as the target void ratio increased, the compressive strength decreased. As the target void ratio increased, strength seems

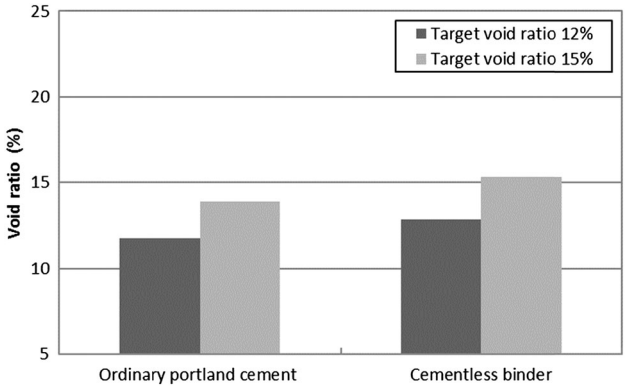

Fig. 8 Void ratio of porous concrete depending on binder type.

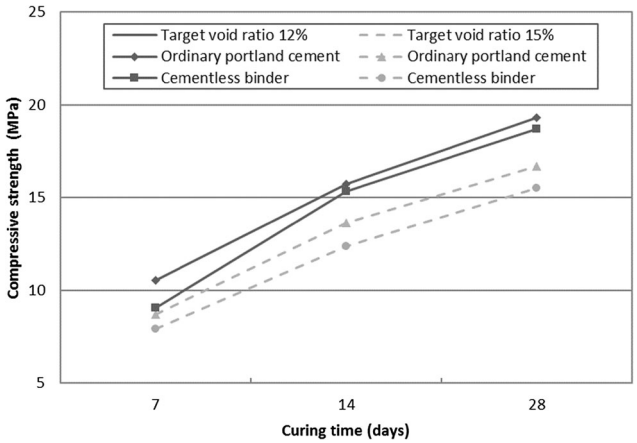

Fig. 9 Compressive strength of the OPC and cementless binder porous concrete with different curing times.

to have decreased due to a decrease in the amount of paste with respect to the amount of unit aggregates. For the same target void ratio, porous concrete using cementless binder tended to decrease in compressive strength in comparison with porous concrete using OPC, but the difference was negligible, at 0.6–1.4 MPa. Meanwhile, under all mixing conditions. The compressive strength of porous concrete was estimated over 15 MPa at all mixing conditions, satisfying 10 MPa which was the specific concrete strength of porous concrete.

3.5 Freezing–Thawing

The freezing–thawing test result of porous concrete according to the type of binder is as shown in Fig. 10. Relative dynamic elastic modulus of concrete using cementless binder was lower than that of porous concrete using OPC. Especially, the relative dynamic elastic modulus of porous concrete decreased to 60 % or less at over freezing–thawing 80 cycles. The porous concrete with cementless binder which has relatively larger void than the porous concrete with OPC features relatively more free moisture transport and relatively more slow formation of hydration products due to the latent hydraulic property such as BFS and FA included in the binder and Pozzolanic reaction (Fu et al. 2011). Since the strength development is delayed due

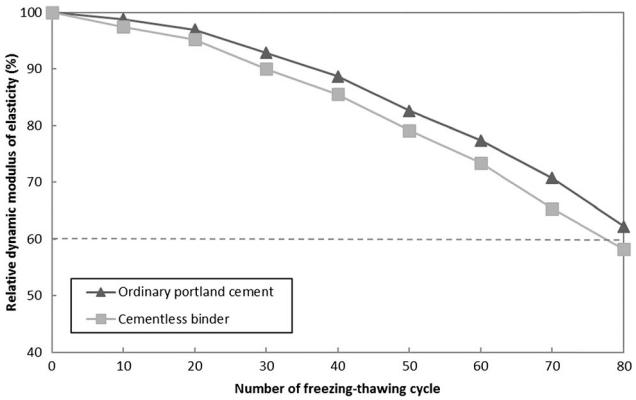

Fig. 10 The relative dynamic modulus of elasticity versus the number of freezing–thawing cycles.

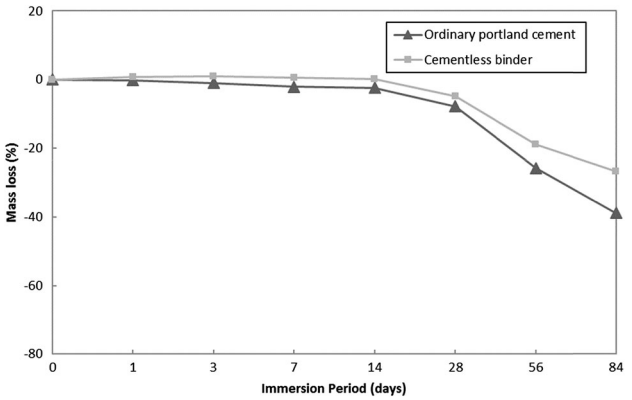

Fig. 12 Mass loss of porous concrete after immersion in 5 % H_2SO_4.

to such reasons, the result showed somewhat deteriorated freezing–thawing resistance.

3.6 Chemical Resistance

Because a large number of continuous voids formed inside the porous concrete, chemical corrosion simultaneously occurred both inside and outside the specimens; chemical resistance was lower in comparison with that of conventional normal concrete. Specimens were produced in accordance with the types of binders, immersed in 5 % HCl and 5 % H_2SO_4 aqueous solutions, and measured to determine their respective mass change rates and surface conditions; the test results are shown in Figs. 11, 12, 13, 14, 15, and 16.

All specimens immersed in the 5 % HCl aqueous solution decreased in mass with the passage of time. In particular, after immersion for 84 days, the mass reduction rate of specimens of porous concrete using cementless binder amounted to 68.53 %, which value is relatively higher than those of specimens of porous concrete using OPC, which had values of 65.46 %. KOH, which is a binder material, engaged in a strong exothermic reaction (-49 kcal/mol) with HCl and generated KCl. Because its solubility in water amounts to 360 g KCl/1 kg H_2O, KCl came to exist in the 5 % HCl aqueous solution in an ionized form. Consequently, there occurred a phenomenon in which KOH hydrates dramatically reacted with HCl, were dissolved, and came to be deleted. Because the surfaces created by the deletion phenomenon exposed CaO to HCl and generated $CaCl_2$, which is a material with high solubility in water, the deletion phenomenon in the specimens was accelerated. For these reasons, porous concrete using cementless binder exhibited a high mass reduction rate.

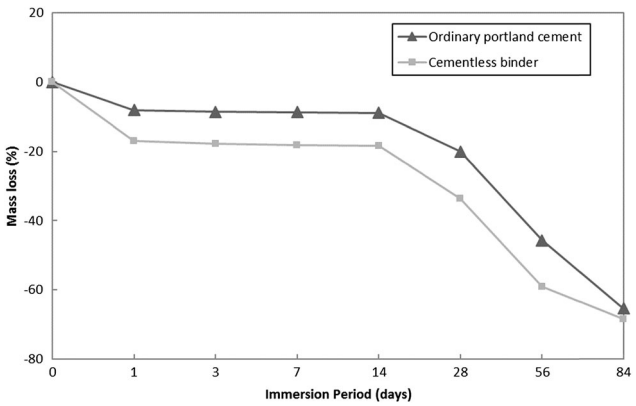

Fig. 11 Mass loss of porous concrete after immersion in 5 % HCl.

Porous concrete using OPC that had been immersed in the 5 % H_2SO_4 aqueous solution continuously decreased in mass with the passage of time, exhibiting a mass reduction rate of 38.87 % after immersion for 84 days. SO_4^{2-} ions infiltrated the porous concrete fabricated using OPC, reacted with $Ca(OH)_2$ generated by the hydration reaction of OPC, and generated $CaSO_4 \cdot 2H_2O$ (separated gypsum), thus causing volume expansion and leading to their elution. In addition, because SO_4^{2-} ions quickly reacted with the $C_3A \cdot CaSO_4 \cdot 12H_2O$ (monosulfate) generated by hydration and continuously generated $C_3A \cdot 3CaSO_4 \cdot 32H_2O$ (Ettringite), bulging failure occurred (Bakharev et al. 2001). In contrast, porous concrete using cementless binder generated K_2SO_4 because of KOH and H_2SO_4 (Gómez-García et al. 2015). Although this reaction is also a strong exothermic reaction (−49 kcal/mol), unlike KCl, which exists as ions, the materials were generated as solid substances and came to exist within all specimens as expansive hydrates. Consequently, while the specimens' masses increased for up to 7 days of immersion, as the immersion period continued, the hydrates became less solid and were gradually deleted from the main bodies, thus leading the mass to decrease to 26.74 % of its original value by the age of 84 days. OPC secured slightly higher chemical resistance performance than cementless binder at 5 % HCl solution, but there was no significant difference. Also, the cementless binder secured a relatively higher chemical resistance performance than OPC at 5 % H_2SO_4 solution. Therefore, it is considered that there would be no problem in the chemical resistance performance if the cementless binder is used in future.

4. Conclusions

In order to effectively recycle the industrial by-product, this study performed the mechanical properties and durability analysis of the porous concrete using cementless binder. The results are as follows:

(a) 7 days (b) 28 days (c) 56 days

Fig. 13 Images of OPC porous concrete after immersion in 5 % HCl.

(a) 7 days (b) 28 days (c) 56 days

Fig. 14 Images of cementless binder porous concrete after immersion in 5 % HCl.

(a) 7 days (b) 28 days (c) 56 days

Fig. 15 Images of OPC porous concrete after immersion in 5 % H_2SO_4.

(a) 7 days (b) 28 days (c) 56 days

Fig. 16 Images of cementless binder porous concrete after immersion in 5 % H_2SO_4.

(1) In cementless binder porous concrete, Gismondine, Hatrurite and Wollastonite, different hydrates from those formed in OPC, were formed. At early ages, Ettringite, $Ca(OH)_2$ and C–S–H gel were formed more slowly in cementless binder than in OPC, but the density of the micro structures and of the structures became similar at the age of 28 days.

(2) The void ratio of porous concrete with cementless binder increased slightly by 1.12–1.42 % from the target void ratio in comparison to the void ratio of

porous concrete with OPC. As a result of evaluating the compressive strength, the compressive strength of porous concrete with cementless binder decreased by comparison to the compressive strength of porous concrete with OPC, but the difference was insignificant at 0.6–1.4 MPa.

(3) As a result of the freeze–thawing test, it was shown that the relative dynamic elastic modulus of porous concrete with cementless binder decreased to 60 % or less at 80 cycle. As a result of the chemical resistance test, it was shown in the 5 % HCl solution immersion test that the porous concrete with OPC produced a slightly higher chemical resistance performance than the porous concrete with cementless binder, and it was shown in the 5 % H_2SO_4 solution immersion test that the porous concrete with cementless binder produced a relatively higher chemical resistance performance than the porous concrete with OPC.

(4) The result of analyzing the characteristics of porous concrete using cementless binder from the studies above shows that there would be no significant impact in terms of securing physical and mechanical performance and durability in comparison to OPC porous concrete. In order to apply the porous concrete using cementless binder, additional studies regarding the application of products such as permeable sidewalk pavers, permeable border blocks and vegetation wall blocks should be carried out in future.

Acknowledgments

This research was supported by Basic Science Research Program through the National Research Foundation of Korea (NRF) funded by the Ministry of Education (No. 2015R1D1A1A01058109).

Open Access

References

Bakharev, T. (2005). Geopolymeric materials prepared using Class F fly ash and elevated temperature curing. *Cement and Concrete Research, 35*(6), 1224–1232.

Bakharev, T., Sanjayan, J. G., & Cheng, Y.-B. (2001). Resistance of alkali activated slag concrete to carbonation. *Cement and Concrete Research, 31*(9), 1277–1283.

Brough, A. R., & Atkinson, A. (2002). Sodium silicate-based, alkali-activated slag mortars: Part I. Strength, hydration and microstructure. *Cement and Concrete Research, 32*(6), 865–879.

Criado, M., Fernández-Jiménezb, A., & Palomob, A. (2010). Alkali activation of fly ash. Part III: Effect of curing conditions on reaction and its graphical description. *Fuel, 89*(11), 3185–3192.

Fu, Y., Cai, L., & Wu, Y. (2011). Freeze–thaw cycle test and damage mechanics models of alkali-activated slag concrete. *Construction and Building Materials, 25*(7), 3144–3148.

Gartner, E. (2004). Industrially interesting approaches to low-CO_2 cements. *Cement and Concrete Research, 34*(9), 1489–1498.

Gómez-García, M. A., Dobrosz-Gómez, I., & Ibarra-Taquez, H. N. (2015). Interaction parameters and (solid + liquid) equilibria calculation for $KCl–H_2O–HCl–C_2H_5OH$, $K_2SO_4–H_2O–H_2SO_4$ and $K_2SO_4–H_2O–C_2H_5OH$ mixed solvent–electrolyte systems. *The Journal of Chemical Thermodynamics, 91*, 427–434.

Japan Concrete Institute, *Research Committee Report for the Establishment of Design and Construction Method for Porous Concrete*, JCI, 2003. (in Japanese)

Juenger, M. C. G., Winnefeld, F., Provis, J. L., & Ideker, J. H. (2011). Advances in alternative cementitious binders. *Cement and Concrete Research, 41*(12), 1232–1243.

Kathirvel, P. (2016) Influence of recycled concrete aggregates on the flexural properties of reinforced alkali activated slag concrete. *Construction and Building Materials, 102*, Part 1, 51–58.

Kumar, S., Kumar, R., & Mehrotra, S. (2010). Influence of granulated blast furnace slag on the reaction, structure and properties of fly ash based geopolymer. *Journal of Materials Science, 45*(3), 607–615.

Lee, B. J., Park, S. B., Kim, Y. Y., & Jang, Y. I. (2012). Experimental study on engineering performance evaluation and field. *Journal of the Korea Concrete Institute, 24*(2), 165–172 (in Korean).

Malhotra, V. M. (2002). Introduction: sustainable development and concrete technology. *Concrete International, 24*(7), 22.

Mehta, P. K. (2001). Reducing the environmental impact of concrete. *Concrete International, 23*(10), 61–66.

Oh, T. K. (2005). A review on the EIA system of each country and its implication. *Journal of the Korea Contents Association, 5*(4), 62–70 (in Korean).

Oh, J. E., Jun, Y. B., Jeong, Y. N., & Jeon, D. H. (2015). Microstructural and strength improvements through the use of Na_2CO_3 in a cementless $Ca(OH)_2$-activated Class F fly ash system. *Cement and Concrete Research, 67*, 215–225.

Pacheco-Torgal, F. (1991). Alkali activated ground granulated blast-furnace slag concrete: preliminary investigation. *Cement and Concrete Research, 21*(1), 101–108.

Park, C. W., & Park, S. K. (2005). Eco-friendly of concrete. *Journal of the Korea Concrete Institute, 20*(6), 24–26 (in Korean).

Park, S. G., Kwon, S. J., Kim, Y. M., & Lee, S. S. (2013). Reaction properties of non-cement mortar using ground

granulated blast furnace slag. *Journal of the Korea Contents Association, 13*(4), 392–399 (in Korean).

Puertas, F., & Fernández-Jiménez, A. (2003). Mineralogical and microstructural characterisation of alkali-activated fly ash/slag pastes. *Cement & Concrete Composites, 25*(3), 287–292.

Wu, S. K., Park, S. J., Kim, M. J., & Son, K. M. (2013) Evaluation and management methodology development for greenhouse gas mitigation measures. Technical report no. 2013–10, The Korea Transport Institute, Ilsan, Korea (in Korean).

Yang, K. H., Hwang, H. Z., Kim, S. Y., & Song, J. K. (2007). Development of a cementless mortar using hwangtoh binder. *Building and Environments, 42*(10), 3717–3725.